



Ship-based lidar measurements for validating ASCAT-derived and ERA5 offshore wind profiles

Hugo Rubio^{a,b}, Daniel Hatfield^c, Charlotte Bay Hasager^d, Martin Kühn^b, and Julia Gottschall^a

^aFraunhofer Institute for Wind Energy Systems IWES, 27572 Bremerhaven, Germany

^bForWind, Institute of Physics, Carl von Ossietzky Universität Oldenburg, Kükersweg 70, 26129 Oldenburg, Germany

^cC2Wind ApS, Vesterballevej 5, 7000 Fredericia, Denmark

^dDepartment of Wind Energy and Systems, Technical University of Denmark, Frederiksborgvej 399, 4000 Roskilde, Denmark

Correspondence: Hugo Rubio (hugo.rubio1@uni-oldenburg.de) and Julia Gottschall (julia.gottschall@iwes.fraunhofer.de)

Abstract.

The accurate characterization of offshore wind resources is crucial for the efficient design and operation of wind energy projects. However, the scarcity of in situ observation in marine environments requires exploration of alternative approaches. For this reason, this study presents a comprehensive comparison between wind profiles derived from the Advanced Scatterometer (ASCAT) satellite observations and the ERA5 reanalysis dataset against ship-based lidar measurements in the Northern Baltic Sea. In order to extrapolate ASCAT observations to wind turbine relevant heights, a long-term correction approach has been implemented. Due to the sensitivity of this method to the accurate characterization of the atmospheric stability, two different approaches were assessed to characterize the stability conditions, showing a great robustness of the methodology employed and leading to noticeable differences only in specific coastal locations. The comparison reveals a close agreement between ASCAT and ERA5 beyond 40 km distance from the coast. Specifically, ASCAT tends to overestimate the mean wind speed derived from lidar measurements, while ERA5 exhibits a consistent underestimation. In terms of vertical accuracy, ERA5 displays a consistent bias of approximately 0.5 m s^{-1} along the profile, whereas ASCAT exhibits a smaller bias within the lower 200 m of the profile. These findings underline the potential and limitations of ASCAT-derived wind profiles and ERA5 for offshore wind characterization.

1 Introduction

Offshore wind energy has experienced significant growth in recent years, and this trend is expected to continue in the coming decade. Forecasts indicate that the world's installed capacity for this technology will increase from 63 GW in 2022 (International Renewable Energy Agency, 2023) to around 370 GW by the end of 2031 (Global Wind Energy Council, 2022). This rapid development of offshore wind farms, coupled with the maturing of floating technology as an alternative to fixed-bottom turbines (Wind Europe, 2021), is accelerating the demand for accurate wind observations in coastal and far offshore areas. Nevertheless, in situ wind observations at turbine-relevant heights in the marine environment are sparse in both time and space due to the constructional limitations and the high installation and operational costs of the traditionally employed meteorological masts (met masts).



Floating lidar systems offer a cost-efficient alternative to offshore met masts (Clifton et al., 2015), thanks to their robustness and reliability (Gottschall et al., 2017; Carbon Trust, 2018), and the potential to increase the flexibility and lower the costs of offshore measurement campaigns. Profiling lidar systems installed in cruising ships, in particular, are capable of providing reliable wind profile measurements over extensive regions. Although the adoption of this technology as an industry standard requires overcoming specific challenges, such as validating these measurements against reference data and quantifying the associated uncertainty (Rubio and Gottschall, 2022), the extensive spatial coverage of ship-based lidar has demonstrated its applicability in various wind-energy relevant activities. In Wolken-Möhlmann and Gottschall (2014), ship-based lidar measurements were used to measure offshore wind farm wakes. In Witha et al. (2019a); Gottschall et al. (2018); Savazzi et al. (2022), ship-borne measurements were used for validating numerical models datasets and in Pichugina et al. (2017); Rubio et al. (2022) for characterizing low-level jets in different offshore regions.

Numerical weather prediction models are commonly used by the industry to obtain wind information in offshore regions where in situ measurements are unavailable. These models provide long-term wind time series at several vertical levels within the boundary layer and with an extensive spatial coverage. However, while numerical models have demonstrated good performance in shallow-water offshore regions compared to in situ measurements (Witha et al., 2019b), they often fail to describe the spatial and temporal variability of wind with sufficient accuracy and detail. This limitation arises from factors such as the inaccurate parameterization of the model variables or the insufficient temporal and spatial resolution of the models' output data. Furthermore, the lack of in situ measurements in deeper offshore regions hinders the validation of these datasets, leading to increased uncertainties in derived wind statistics for such locations.

To overcome the limitations of in situ measurements and numerical models, satellite remote sensing devices have emerged as a potential alternative for characterizing ocean winds and climate over large areas, capturing the wind variability with a temporal coverage of over 15 years. For this reason, several studies have focused on characterizing offshore wind resources using satellite measurements (Remmers et al., 2019; Ahsbahs et al., 2020; Hasager et al., 2020). One of the most well-known satellite-based instruments used for wind energy purposes is the Advanced Scatterometer (ASCAT), mounted onboard the European Space Agency's MetOp series of polar orbiting satellites. ASCAT provides global ocean wind measurements with a resolution down to 12.5 km. However, the application of satellite measurements for wind energy purposes has been limited by three main factors. First, the limited temporal resolution of polar-orbiting satellites restricts wind measurements to a few fixed times per day, rendering these products unable to fully capture the diurnal wind speed variability. Second, satellite measurements are provided at 10 m above the sea surface, requiring the implementation of extrapolation methods to derive wind information at turbine operating heights. Lastly, the trustworthiness of satellite retrievals remains a knowledge gap, due to the lack of available in situ datasets for validation especially in deep water regions.

The Baltic Sea is an area of great interests for offshore wind development due to its strong and consistent wind resource, relatively shallow water depths, and proximity to large population centres. However, it is a complex and dynamic environment, characterized by strong land-sea interactions and atmospheric processes that generate significant wind speed and direction gradients, as well as specific mesoscale phenomena such as sea breezes or low-level jets (Smedman et al., 1997). Consequently, the Baltic Sea has been extensively studied in the previous literature aiming to accurately characterize the available wind



resource in the region. In Svensson (2018), numerical models and different types of measurements were used to characterize mesoscale processes. In Hasager et al. (2011); Karagali et al. (2014); Badger et al. (2016); Karagali et al. (2018), wind resource statistics were derived from satellite measurements. In Hatfield et al. (2022), ship-based lidar measurements were extrapolated down to 10 m and compared against observations from FINO2 met mast and ASCAT, as well as against the New European Wind Atlas (NEWA) mesoscale simulations.

The objective of this paper is to assess the accuracy of ASCAT-derived wind speed profiles in the nearshore and offshore locations of the Northern Baltic Sea by conducting a comprehensive comparison against ship-based lidar measurements. Additionally, the numerical model output data from the ECMWF Reanalysis 5th generation (ERA5) is included in this analysis to evaluate and highlight the different wind profiles obtained through the application of the different datasets. To accomplish this comparison, we employ the long-term stability correction approach presented in Kelly and Gryning (2010) and implemented in Badger et al. (2016) to derive wind profiles from the ASCAT 10 m measurements. For this, we utilize the stability information from ERA5 and compare two different collocating methods to evaluate the potential influence of the limited temporal resolution of satellite overpasses in the ASCAT extrapolated profiles. Furthermore, we introduce a novel collocation strategy for comparing ASCAT-derived and ERA5 profiles against the ship-mounted lidar observations, which has not been previously reported. To the authors' knowledge, this study represents the first comprehensive comparison of ASCAT wind profiles extrapolated to wind turbine operational heights against non-stationary in situ measurements, covering a wide horizontal extent that extends from nearshore to offshore locations. Therefore, this work may contribute significantly to a better understanding of the reliability and accuracy of satellite measurements for offshore wind characterization at wind energy relevant heights.

The paper is structured as follows. Section 2 presents the ship-based lidar measurement campaign, as well as the ERA5 and ASCAT datasets used in this study, along with the implemented data processing methods. This section also provides a detailed description of the long-term stability correction method used for ASCAT wind extrapolation and the collocation procedure employed for the comparison of the three datasets. Section 3 contains the main results obtained in this investigation. Discussion of these findings and main extracted conclusions are included in Sections 4 and 5, respectively.

2 Data and Methods

This section describes the three datasets used throughout this work. In addition, the methodology used for processing the different datasets is detailed, as well as the methodology to extrapolate ASCAT winds and for their comparison against the ship-based lidar measurements.

2.1 Ship-based lidar measurements

The ship-based lidar observations used in this study were acquired through the execution of a novel ship-based lidar measurement campaign designed and conducted by the Fraunhofer Institute for Wind Energy Systems IWES (Germany). In this campaign, a wind lidar profiler was installed on-board the ferry ship *Stena Gothica*, operated by the company Stena Line, along the regular route between the harbours of Nynäshamn (Sweden) and Hanko (Finland) in the Northern Baltic Sea. Figure 1a



shows the average route of *Stena Gothica* ferry; only small deviations from this route took place during the execution of the campaign. The ship covers this route on a daily basis, travelling from one harbour to the other within one day, and travelling back the following day. Additionally, the frequency distribution of the ship location versus the hour of the day is presented in Fig. 1b. As can be observed, the ship typically remains at the harbours during the central hours of the day (from 7:00 to 17:00 UTC), while it travels from one harbour to the other between the evening and the early morning. The consistent relationship between the time of the day and the ship's location is a particular aspect of these sort of campaigns, already observed in similar experiments such as the NEWA Ferry Lidar Experiment (Gottschall et al., 2018; Rubio et al., 2022).

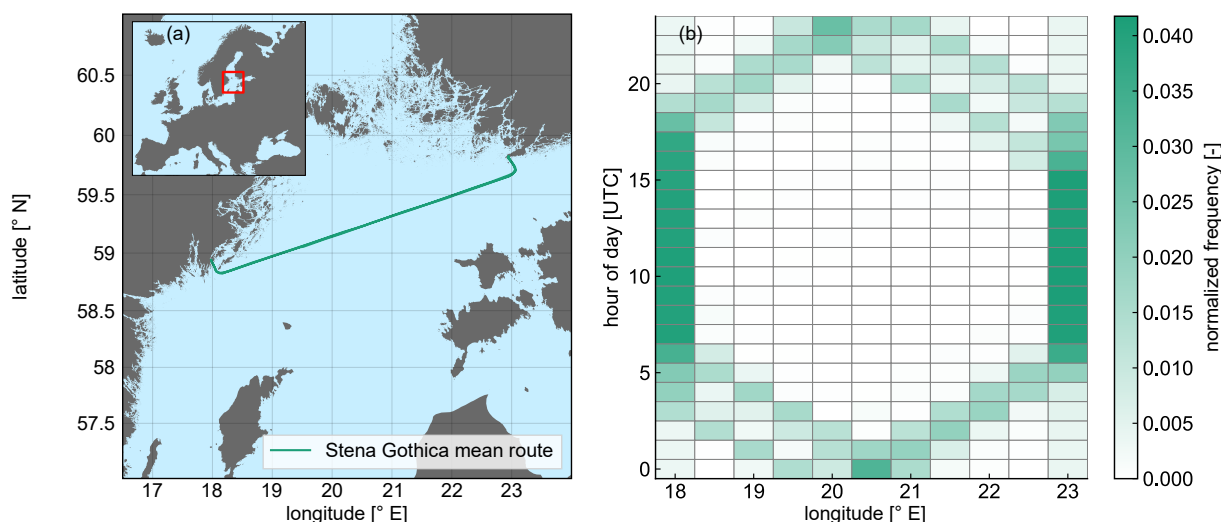


Figure 1. On the left panel, the mean route of the *Stena Gothica* ferry ship during the execution of the campaign. On the right, 2D histogram of the location of the ship depending on the hour of the day and the longitude of its position.

The campaign took place from 28 June 2022 to 21 February 2023 and as in Gottschall et al. (2018), the Fraunhofer IWES's in-house developed ship-based lidar system was used. This is composed by a vertical profiling Doppler lidar WindCube WLS7 v2, from the manufacturer Vaisala, configured to measure at twelve different height levels ranging from 60 to 270 m above sea level (ASL). Apart from the lidar device, the integrated ship-based lidar system includes a motion recording unit to track the vessel motions and positions (attitude and heading reference sensor and a satellite compass) and a meteorological station to record the main meteorological parameters, including temperature, pressure, relative humidity, and precipitation.

As in previous ship-based lidar campaigns, a ship-motion compensation algorithm was implemented in order to take the motions effects out of the measurements. For this, the motion information recorded by the system is used in combination with the wind lidar measurements, using a simplified motion correction algorithm (Wolken-Möhlmann and Gottschall, 2014). This algorithm considers the translational ship velocity and orientation, ignoring vessel tilting due to its negligible influence on the results. Additionally, lidar measurements with carrier-to-noise ratio (CNR) values below -23 dB were rejected from the final database, following the manufacturer's recommendation to strike a balance between data availability and accuracy. Subsequently, lidar measurements and motion information (i.e. ship coordinates) were averaged into 10-minute mean values.



Figure 2 provides some insights into the measured data during the campaign. In the first panel, the longitude binned wind speed can be observed, along with the normalized frequency of 10-minute average recordings at each longitude bin. The lowest wind speed corresponds to the longitude bin encompassing the Swedish harbour, with an average velocity of around 6.6 m s^{-1} . This specific location, Nynäshamn harbour, can be considered onshore due to its intricate topography, characterized by numerous small islands and hills that slow down the wind flow. In contrast, the remaining locations are characterized as offshore sites, presenting mean wind speeds above 8.5 m s^{-1} , with the highest mean speed observed at the Hanko harbour.

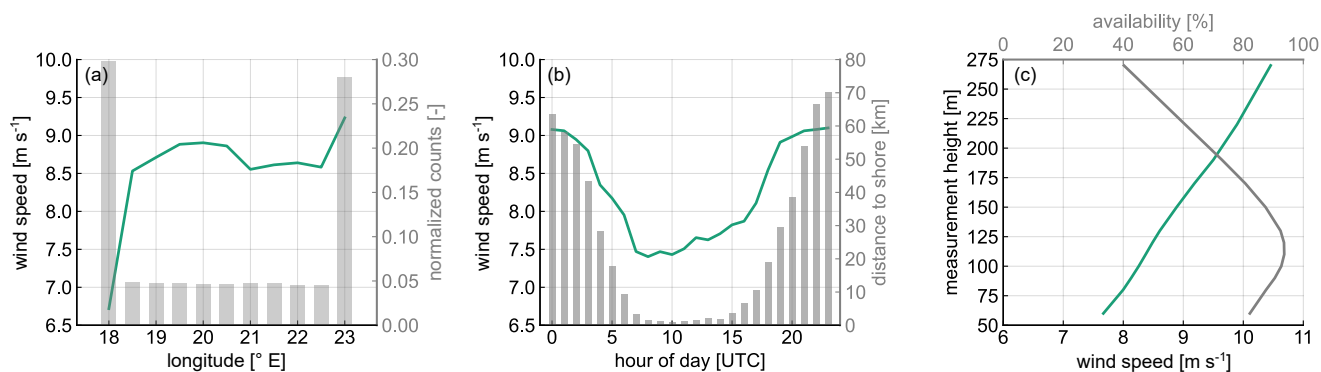


Figure 2. Summary of lidar measurements. (a) Mean wind speed per longitude (green line) and normalized number of 10-min counts per longitude (bars). (b) Wind speed daily cycle (green line) and mean distance to shore per hour (bars). (c) Mean wind speed profile (green line) and mean availability during the campaign time extent per measurement height ASL (grey line).

Figure 2b illustrates the wind speed daily cycle (represented by the solid line) and the mean distance to the shore per hour (represented by the bars). The minimum wind speeds occur during the central hours of the day, coinciding with the period when the ship is mainly located at the two harbours. Despite Hanko harbour typically presents stronger wind speeds, the considerably lower wind velocities measured at Nynäshamn and the higher frequency of observations at this site (refer to Fig. 2a) result in a noticeable fall in the average wind speed during these hours. In contrast, the highest wind speeds are observed during the night and the early morning, when the ship is typically in transit between the two harbours.

Finally, Fig. 2c shows the mean wind speed along the measured wind profile (represented by a green line) together with the total availability profile of the lidar over the campaign (represented by a grey line). As can be observed, there is a pronounced increase of the mean wind speed with height, going from 7.6 m s^{-1} at 60 m height to 10.4 m s^{-1} at the top measurement height. The availability profile shows maximum values above 90 % within the range of 80 to 130 m ASL range. Beyond 130 m, the availability drops rapidly with the height as a consequence of the very clean air and the low concentration of aerosols in the region and period of study. The decrease in availability at the lower levels is explained by the lidar device's focus distance of around 120 m ASL. Moving further below or beyond this distance results in lower CNR values and consequently, measurements are filtered out of the dataset when CNR falls below the -23 dB threshold.



Therefore, the ship-based lidar measurements provide valuable information about the spatio-temporal variability of wind speed in the Northern Baltic Sea region. The data captured the unique characteristics of the study area, including the influence of the different locations and the diurnal wind speed patterns associated with the ship's travel between the harbours.

2.2 ASCAT

135 The Advanced Scatterometer (ASCAT) is a space-borne remote sensing instrument which measures radar backscatter from the Earth's surface in the microwave frequency range (Martin, 2014). ASCAT was launched by the European Space Agency's (ESA) onboard the Meteorological Operation (MetOp) satellites, developed and operated by the European Organization for the Exploitation of Meteorological Satellites (EUMETSAT) (Verhoef and Stoffelen, 2019). MetOp-A was the first launched satellite in October 2006, followed by MetOp-B in September 2012 and by MetOp-C in November 2018. ASCAT has an
140 effective swath width of 512.5 km with a nadir gap of 700 km, resulting in a temporal resolution of 1 to 3 overpasses daily considering both the ascending and the descending trajectories, depending on the time period and location (latitude). The number of ASCAT overpasses in the Northern Baltic Sea region during the execution of the measurement campaign is presented in Fig. 3a, whereas the diurnal distribution of the overpasses is shown in Fig. 3b.

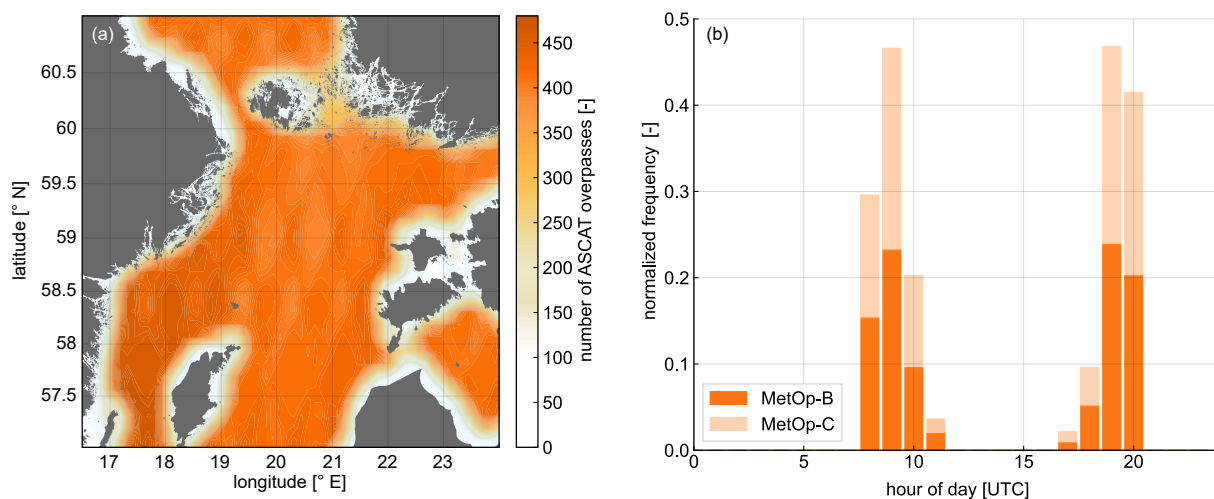


Figure 3. (a) Number of ASCAT overpasses during the duration of the campaign. (b) Normalized frequency of ASCAT overpasses per hour of the day.

145 The ASCAT scatterometer is an active microwave radar that measures the backscatter power from transmitted pulses operating in the C-band frequency of 5.255 GHz. These measurements are unaffected by cloud cover and rain. The received backscatter is related to the surface roughness of the observed area, being zero when having completely smooth surfaces and simultaneously increasing with the roughness. This backscatter signal is used to calculate the normalized radar cross-section (NRCS, σ_0), defined as the ratio of the received and the transmitted power, that depends on the radar settings, the atmospheric attenuation, and the ocean surface characteristics (Chelton et al., 2001). From NRCS and through the application of an empiri-



150 cally derived geophysical model function (GMF), the sea surface winds are calculated. These empirical models are calibrated
using in situ measurements of wind speed from buoys and other sources, and are validated using independent measurements
from other satellite instruments and numerical models (Hersbach et al., 2007; Hersbach, 2008; Verspeek et al., 2012). The
current GMF used by ASCAT is the CMOD7 (Stoffelen et al., 2017), which was developed by the ESA specifically for its use
with C-band scatterometers.

155 ASCAT provides wind speed and direction measurements at 10 m above the sea surface, with a global coverage and available
spatial resolutions of 12.5 km and 25 km (de Kloe et al., 2017). For this study, the higher spatial resolution data has been
selected, since it has shown better performance in previous studies when validated against in situ measurements (Verhoef and
Stoffelen, 2013; Carvalho et al., 2017). This dataset is processed and distributed by EUMETSAT Ocean and Sea Ice (OSI)
Satellite Application Facility (SAF) and by the Advanced Retransmission Service (EARS). Both of these are implemented at
160 the Koninklijk Nederlands Meteorologisch Instituut (KNMI) and were downloaded for this study using the Copernicus Marine
Data Service (CMS) (product id: WIND_GLO_WIND_L3_NRT_OBSERVATIONS_012_002).

The implemented data process for the ASCAT measurements is the following. Firstly, a coordinate transformation was
applied to transfer ASCAT coordinate points from the bottom left corner of each grid box to the centre of the box. Subsequently,
a quality check was conducted by filtering out data based on the quality flags provided directly by the CMS (E.U. Copernicus
165 Marine Service Information (CMEMS). Marine Data Store (MDS)). To address the issue of coastal contamination and mitigate
the influence of excessively high mean wind speed values in ASCAT grid cells near the coast (Stoffelen et al., 2008; Lindsley
et al., 2016), an interquartile range (IQR) outlier detection method was employed. This method identifies grid boxes with
significantly higher values of wind speed and masks them out from the analysis. By applying the IQR outlier detection, the
impact of coastal contamination on the wind speed data is minimized, leading to more accurate and reliable results in nearshore
170 areas.

2.3 ERA5

ERA5 (ECMWF Reanalysis 5th generation) is the latest global atmospheric reanalysis produced by the European Centre for
Medium-Range Weather Forecasts (ECMWF) (Hersbach et al., 2020). ERA5 replaces the previous reanalysis ERA-Interim
(Dee et al., 2011) and it is based on the latest version of the Integrated Forecasting System (IFS) model IFS Cycle 41r2.
175 ERA5 provides hourly estimates of a wide range of atmospheric, land surface and oceanic variables with a $0.25^\circ \times 0.25^\circ$
latitude-longitude grid resolution, covering the period from 1950 to present. Additionally, ERA5 used 137 model (pressure)
levels extending from the surface level to the top of the atmosphere at 0.01 hPa or around 80 km height. ERA5 is produced
using an assimilation scheme based on the four-dimensional variational (4D-Var) system (Bonavita et al., 2016). This method
integrates modelled data from the IFS with observational data from a range of sources such as satellites, radiosondes, and
180 aircrafts widespread across the world.

For this study, the u and v wind components were downloaded for the 10 lowest model levels to calculate the horizontal wind
speed and direction. Additionally, the surface sensible heat flux, temperature of air at 2 m above the surface, and friction velocity
parameters were also downloaded for deriving the atmospheric stability information required for ASCAT winds extrapolation



(see Section 2.4). Furthermore, the ERA5 data were re-gridded to match the ASCAT wind speed maps resolution (0.125° latitude and longitude) using bilinear interpolation.

2.4 Satellite long-term extrapolation

One of the main limitations for the application of satellite remote sensing measurements in the field of wind energy is that they provide wind information only at surface level. Consequently, vertical extrapolation methods need to be implemented to obtain wind information at wind turbine hub heights. Several methodologies to vertical satellite extrapolation have been explored in previous literature. Capps and Zender (2009, 2010) used 10-m wind measurements from QuickSCAT to estimate the global wind power potential at various vertical levels. For this, the Monin-Obukhov similarity theory (MOST) was implemented for the atmospheric stability correction of the vertical wind profile, using data from a global ocean-surface heat flux product and reanalysis data. Doubrava et al. (2015) employed the equivalent neutral winds from QuickSCAT and SAR along with a neutral logarithmic profile to calculate a wind atlas in the Great Lakes region. Badger et al. (2016) and Hasager et al. (2020) extrapolated SAR and ASCAT surface winds using the long-term stability correction presented in Kelly and Gryning (2010), which is based on a probabilistic adaptation of the MOST-based wind profile. Finally, Hatfield et al. (2023) developed a machine-learning model to extrapolate ASCAT winds to wind turbine operating heights, employing 12 years of satellite wind observations in conjunction with near-surface atmospheric measurements at FINO3, and comparing the output wind profiles against in situ measurements and numerical model data.

In this study, we employ the approach used by Badger et al. (2016) and Hasager et al. (2020) to calculate the extrapolated ASCAT wind profiles. This method involves a long-term correction of atmospheric stability effects, obtained from the numerical model dataset ERA5, along with an adaptation of the MOST to vertically extrapolate the satellite wind measurements. The long-term stability correction derived from this methodology can exhibit positive or negative values depending on the considered height, as it combines both stable and unstable terms. Conversely, when applying stability correction factors to instantaneous wind speed measurements, the stable or unstable terms are applied separately.

Compared to the approach of instantaneous stability correction, the long-term stability correction enables to circumvent the computation of wind speeds under stability conditions and heights that fall out of the validity range of the MOST model. MOST is specifically designed to describe turbulent fluxes within the surface layer (Lange et al., 2004; Högström et al., 2006), and it has limitations when analysing data on an instantaneous basis, particularly under stable conditions. The long-term adaptation of MOST can effectively be applied up to turbine operating heights, since the long-term stability correction falls within the range where MOST is applicable. In neutral and unstable conditions, MOST can be successfully employed within the lower 200 meters of the vertical profile (Peña et al., 2008). Furthermore, and although previous literature highlighted the good performance of data-based extrapolation methods (Optis et al., 2021; de Montera et al., 2022; Hatfield et al., 2023), the limited time extension of the measurement campaign results in an insufficient amount of data to implement these approaches in this study. Otherwise, a relevant drawback of the long-term correction is that the information provided by the individual wind speed samples is neglected, disguising the potential influence of particular mesoscale effects that modify the average wind profile.



The implementation of the long-term correction approach is described below. This is individually executed for each of the ASCAT grid points by using the stability information from the ERA5 corresponding location. As a result of this process, one
 220 ASCAT-derived mean profile is calculated for each grid point.

The atmospheric stability can be directly accounted for by estimated the Obukhov length L parameter, calculated as:

$$L = -\frac{\overline{T}u_*^3}{\kappa g \overline{w'\theta'_v}} \quad (1)$$

where \overline{T} is the air temperature, u_* is the friction velocity, κ is the von Kármán constant (≈ 0.4), g the Earth's gravitational acceleration, $\overline{w'\theta'_v}$ the kinetic virtual heat flux, where w' is the vertical component of the wind speed, and θ'_v is the virtual
 225 potential temperature. The temporal means are denoted by overbars, while fluctuations around the mean value are indicated by primes. Accurate measurements of heat and momentum fluxes require three-dimensional observations from high-frequency sonic anemometers. However, since we wish to develop an extrapolation method independent from in situ measurements, the mean temperature and heat fluxes in Eq. (1) are replaced by the ERA5 parameters air temperature at 2 m and surface
 230 Obukhov length $1/L$ denote stable atmospheric conditions, negative values indicate unstable conditions, and values around 0 indicate near-neutral stratification.

According to the formulation described in Kelly and Gryning (2010), the probability density function P of $1/L$ can be estimated as:

$$P(L^{-1}) = n_{\pm} \frac{C_{\pm}}{\sigma_{\pm}} \frac{\exp\left[-(C_{\pm}|1/L|/\sigma_{\pm})^{2/3}\right]}{\Gamma[1+3/2]} \quad (2)$$

where the subscripts + and - indicate the stable and unstable portions of the distribution, respectively; n_{\pm} are the fractions of occurrence of each portion, C_{\pm} are semi-empirical constants, and σ_{\pm} are the scale of variations in $1/L$, based on the long-term standard deviation of the surface heat flux and the average of the cube of the friction velocity, as indicated in the equation
 below:

$$\sigma_{\pm} = \frac{g}{\langle \overline{T} \rangle} \sqrt{\frac{\langle (\overline{w'\theta'_v} - \langle \overline{w'\theta'_v} \rangle_{\pm})^2 \rangle}{\langle u_*^3 \rangle}} \quad (3)$$

As for Eq. (1), we replace the mean temperature and heat fluxes with the corresponding parameters provided by ERA5.

In this study, the values for the C_{\pm} constants have been set to 6 and 4 for the stable and unstable portions, respectively. Although previous studies focused on different datasets have used other values (e.g. both set to 3 in Badger et al. (2016); and $C_+ = 5$ and $C_- = 12$ in Optis et al. (2021)), the selected values in this study were specifically chosen to ensure the derivation of a representative probability density function of the atmospheric stability across all the ASCAT grid boxes along the entire
 245 ship route. Furthermore, identical values of C_{\pm} were applied to all ASCAT grid points.



Finally, the long-term stability correction of the mean long-term wind profile at a specific height z is calculated as:

$$\Psi_m^* = -n_+ \frac{3\sigma_+}{C_+} b' z + n_- f_- \quad (4)$$

where b' is calculated as

$$b' = \frac{b}{\Gamma[1 + 3/2]} \quad (5)$$

250 with $b = 4.7$ coming from the standard MOST formulation for stable conditions $\Psi_m = bz/L$ (Stull, 1988). Analogously, f_- is derived from the standard MOST formulation for unstable conditions (see (Kelly and Gryning, 2010) for the exact formulation of f_-).

To evaluate the potential influence of the discretized temporal frequency of ASCAT overpasses, and therefore, the effect of the available stability information in the derivation of the long-term stability correction factor, two different approaches
 255 have been compared. First, for the so-called collocated approach, only ERA5 stability information collocated in time with the ASCAT overpasses is considered. For the second approach, all ERA5 stability information from the whole duration of the campaign is used. The normalized probability density functions of atmospheric stability ($1/L$) derived from ERA5 at two different locations along the ship route is shown in Fig. 4, together with the theoretical distribution calculated from Eq. (2) for the two considered approaches.

260 As observed, considering the stability information from the full campaign results in a better theoretical distribution compared to the collocated approach. Although the difference is minimal at the harbour site, it is more pronounced at the offshore location, where a significant underestimation of unstable stability occurrence is observed. The harbour site presents a rather symmetric distribution around zero, meaning that both unstable and stable atmospheric conditions are equally represented. However, the offshore site exhibits a higher occurrence of unstable conditions, compared to the stable side of the curve. Section 3.1 presents
 265 additional results on this matter and evaluates the differences in the obtained ASCAT wind profiles between the two approaches.

Finally, the extrapolated wind speed at any desired height z can be calculated from Eq. (6) by introducing the long-term stability correction Ψ_m^* obtained from Eq. (4):

$$U(z) = \frac{\langle u_* \rangle}{\kappa} \left[\ln \left(\frac{z}{\langle z_0 \rangle} \right) - \Psi_m^* \right] \quad (6)$$

2.5 Collocation procedure

270 The comparison of gridded datasets (ERA5 and ASCAT) against the non-stationary measurements from the ship-based lidar system requires the implementation of a collocation methodology to ensure a fair comparison. Previous studies have already conducted comparison between gridded data and ship-based lidar measurements (Witha et al., 2019b; Hatfield et al., 2022; Rubio et al., 2022). However, unlike previous literature that focuses on time-space collocated comparisons, in this study, ship-based lidar measurements are compared against the mean wind profiles calculated for each of the grid points from the gridded

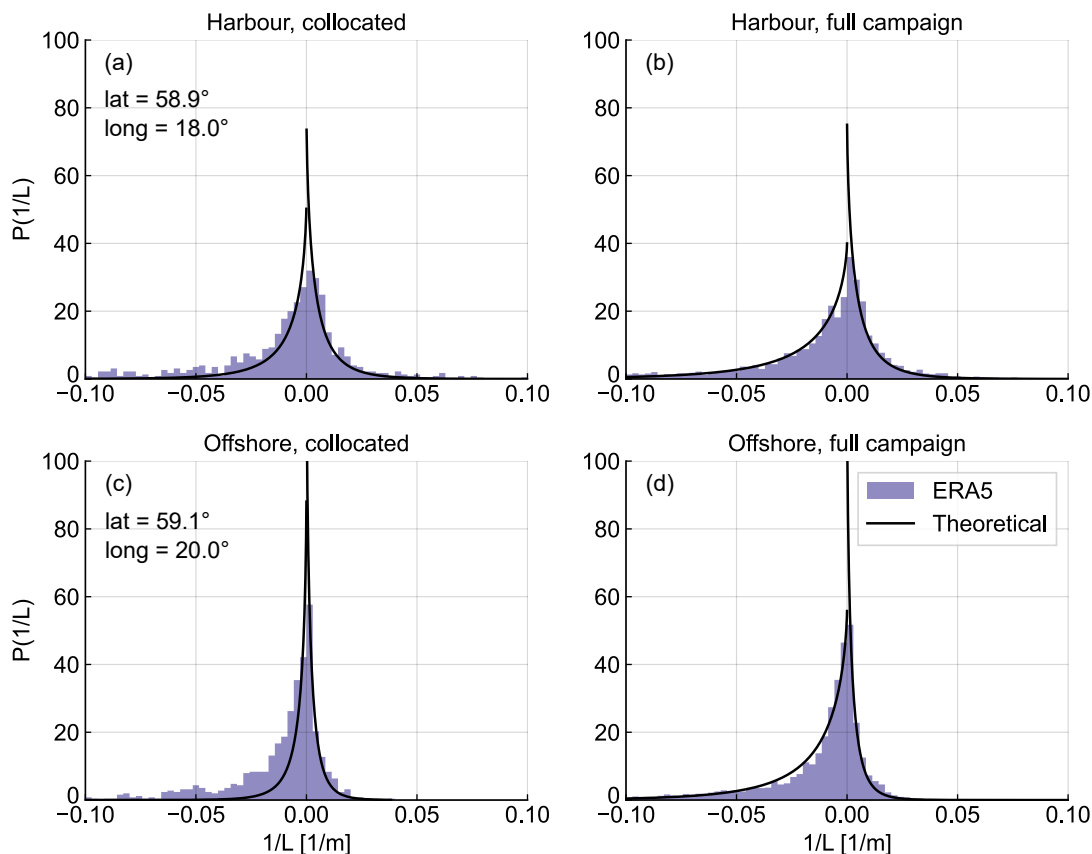


Figure 4. Normalized probability density functions of inverse Obukhov length $1/L$ from ERA5 and theoretical distributions calculated from Eq. (2). Results are shown for two grid points, one offshore site (panels (c) and (d)) and one location near Nynäshamn harbour (panels (a) and (b)). The coordinates of these sites are indicated in panels (a) and (c), respectively.

275 datasets. Consequently, a novel methodology for collocating and comparing the mean gridded and lidar-measured wind profiles has been developed and is briefly introduced in this section.

After applying the coordinate transformation and re-gridding procedures explained in Sections 2.2 and 2.3, both datasets are gridded with an identical discretization, featuring a horizontal resolution of $0.125^\circ \times 0.125^\circ$ and the grid points located at the centre of the grid boxes, as shown in Fig. 5. For each grid box, the ERA5 mean profile is calculated for the period of the measurement campaign, while the mean ASCAT profile is obtained using the procedure described in Section 2.4. To obtain
280 the mean lidar profiles for comparison, the 10-minute average ship position information is utilized to identify all the 10-minute lidar measurements captured within each grid box. Subsequently, the mean lidar profile for each grid point is calculated by averaging all the 10-minute measurements detected in the corresponding grid box. This enables the comparison of all ERA5 and ASCAT grid boxes with their respective mean wind profiles against the collocated "gridded" lidar mean profile. It should



285 be noted that grid boxes with less than 24 hours of lidar data available (equivalent to 144 10-minute samples) are excluded from the comparison. The procedure is summarized in Fig. 5, where example ship coordinates are depicted as coloured dots, corresponding to the colour of the grid box used for deriving the mean profile.

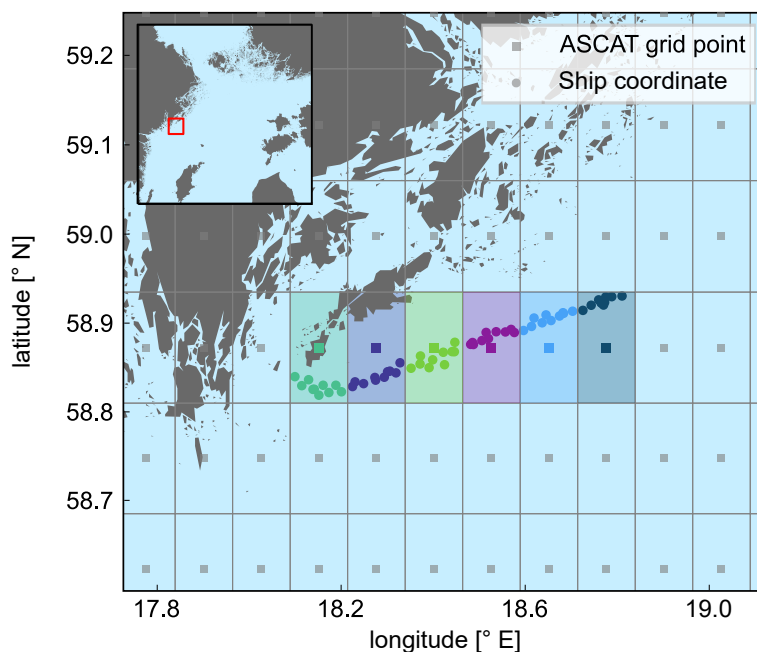


Figure 5. Collocation procedure sketch illustrating the comparison of lidar-measured wind profiles against ERA5 and ASCAT profiles. The grey grid represents the ASCAT and ERA5 grid boxes after the coordinate transformation of ASCAT and the ERA5 re-gridding procedure. For each coloured grid box, all lidar measurements performed within that area (depicted as dots of the corresponding colour) are averaged to calculate the corresponding lidar profile.

3 Results

The main results of this study are presented in this section. Firstly, the influence of the approach employed to derive the long-term stability correction in the extrapolated ASCAT profiles is assessed. Later, a comparative analysis between the ERA5 and ASCAT winds is conducted within the Northern Baltic Sea region. Afterwards, wind speed profiles obtained from ASCAT and ERA5 are compared against the lidar measured profiles to investigate their performance at different vertical and horizontal constraints.

In order to validate the wind profiles derived from ASCAT and ERA5 against the lidar in different locations, these comparisons are performed at the six different locations indicated in Fig. 6. The selection of these locations aims to represent the different wind conditions along the route, including locations at the two harbours, from a short distance to the shore as well as far offshore sites.

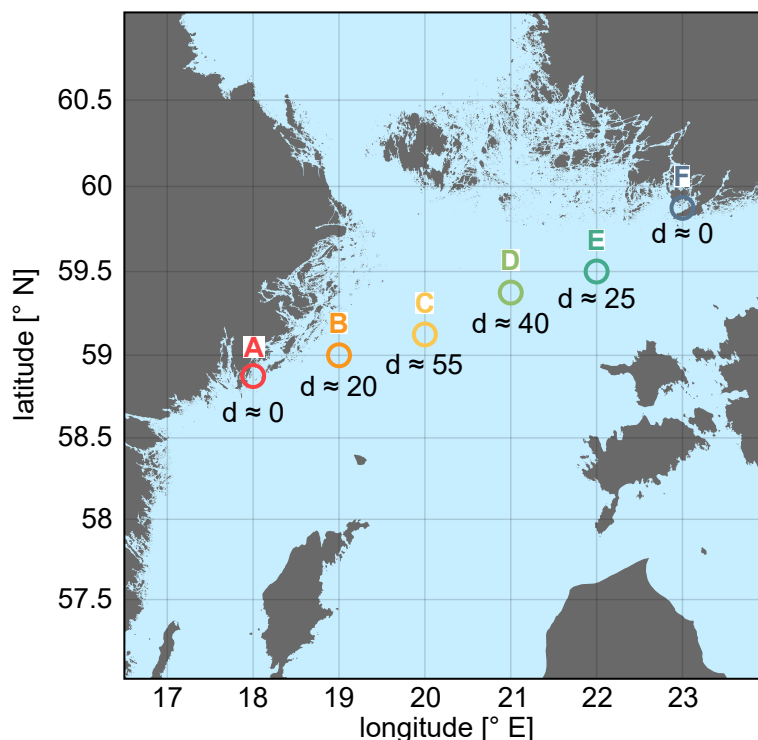


Figure 6. Six locations used for the comparison of the datasets. The approximate distance to the nearest shore is indicated, in km, below of each site.

3.1 Influence of stability information in ASCAT profiles

As explained in Section 2.4, two different approaches have been considered for the characterization of the stability from ERA5 parameters and the corresponding derivation of the long-term stability correction. This section investigates the effects of both approaches in the obtained ASCAT wind profiles.

Figure 7 illustrates the difference in wind speed at a height of 100 m obtained from the collocated approach compared to the full campaign approach. The wind speed discrepancy remains minimal across the vast majority of the study area, particularly along the area covered by the ship track. Within most of the sea area, the collocated approach displays slightly lower mean wind speeds, with notable differences reported in areas near the shore and reaching a maximum wind speed bias of approximately 0.4 m s⁻¹. Notably, the region surrounding the Swedish harbour of Nynäshamn exhibits the greatest difference in wind speed.

The underestimation associated with the collocated approach can be attributed to three primary factors. First, the coastal contamination of near shore areas leads to the removal of some ASCAT overpasses for data quality reasons, leading to a reduced number of ASCAT observations in this areas. Consequently, the insufficient number of valid wind speed measurements obtained from the collocated approach introduces a biased representation of the prevailing stability conditions during the campaign period. Secondly, the temporal discretization of ASCAT overpasses, which occur at roughly the same time each day,



influences the resulting main stability distribution "seen" by the collocated approach. This is illustrated in Fig. 8, depicting the daily cycle of the mean stability ($1/L$) at the six locations presented in Fig. 6. As can be observed, the collocated approach yields a more unstable distribution of the stability conditions near the Nynäshamn harbour (red line) due to the pronounced
315 instability in the morning. This results in a lower wind speed compared to the full campaign approach, as can be derived from Eq. 4. In contrast, the other locations do not exhibit such pronounced daily stability cycles, and therefore, smaller differences are reported between the two approaches. Finally, as mentioned in Section 2.4, the same values of the semi-empirical constant C_{\pm} are assumed for the entire region, instead of using a site-specific definition of these constants. Therefore, the suitability of the selected values may not be optimal for certain locations, leading to an anomalous theoretical representation of the empirical
320 atmospheric distribution.

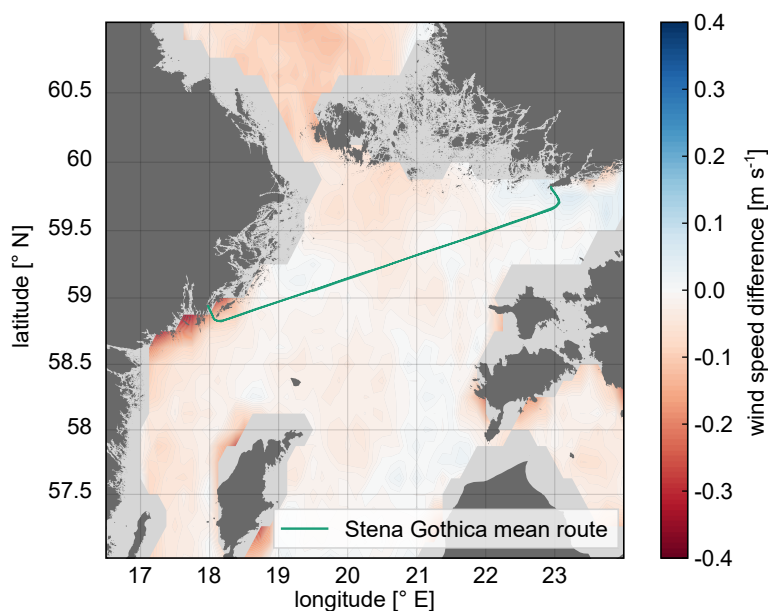


Figure 7. Mean wind speed difference at 100 m height between the collocated and full campaign approaches.

Both strategies for calculating the stability correction factor and the corresponding wind profiles demonstrate a high level of agreement, except for some nearshore locations. This highlights the robustness of the employed methodology and indicates that the dataset size allows for an accurate characterization of atmospheric stability conditions during the campaign and along the entire ship track. Given the similarity of the wind profiles obtained using both approaches, and for the sake of clarity and
325 conciseness, the upcoming sections will only consider the full campaign approach. This approach is expected to provide more representative wind profiles along the complete ship route.

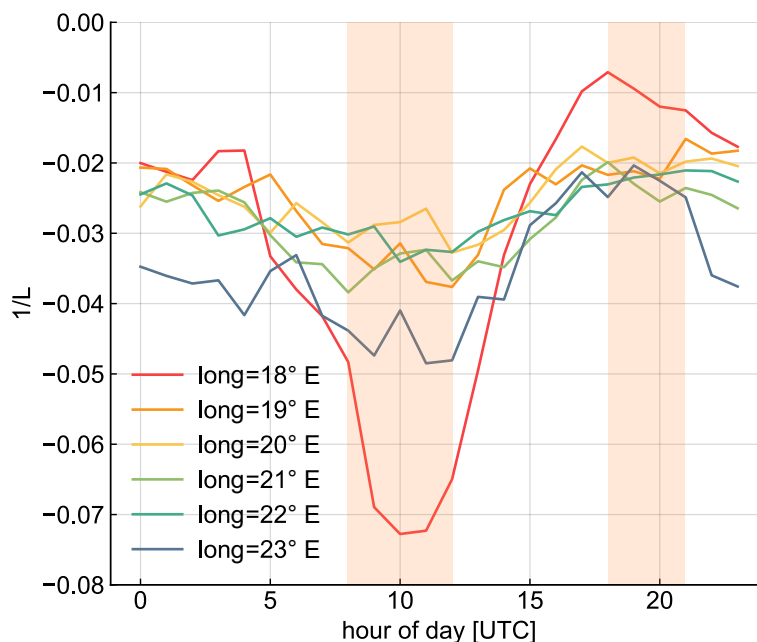


Figure 8. Daily cycle of the stability parameter ($1/L$) at the six evaluated locations. The orange shadows indicate the time periods when ASCAT overpasses are available and therefore, considered for the stability characterization in the collocation approach.

3.2 ASCAT-derived vs ERA5 wind speeds

The offshore mean wind speeds based on ASCAT and ERA5 in the Northern Baltic Sea region at 10 m and 100 m heights are compared in Fig. 9. For an easier comparison, only grid points where ASCAT data is available are included and the same colour scale is used for the four plots.

330

Both datasets consistently show higher wind speeds at 100 m than at 10 m height. The overall mean wind speeds at 10 m are 7.6 m s^{-1} and 7.2 m s^{-1} for ASCAT and ERA5, respectively. At 100 m, these values increase to 9.3 m s^{-1} for ASCAT and 8.7 m s^{-1} for ERA5. When looking at the spatial variation shown by the two datasets at 10 m, ERA5 exhibits higher mean wind speeds in the areas farthest from the shore at 10 m, with a progressive decrease as the coast is approached. However, and although

335

ASCAT also shows higher wind speeds in the middle of the basin, the closest areas to the shore still present considerably higher values of wind speed compared to ERA5. The reason for this is that, despite the filtering process for the ASCAT dataset, the coastal contamination still affects ASCAT measurements, leading to excessively high mean values in nearshore areas.

The effect of coastal contamination in the ASCAT map is particularly visible in the 100 m height map, where the highest mean wind speeds are located along the perimeter of the region with available data. The stronger impact of coastal contamination at 100 m can be attributed to the inaccurate characterization of stability conditions by ERA5 in nearshore locations due to its coarse horizontal resolution and limited ability to resolve fine-scale atmospheric features in these regions.

340

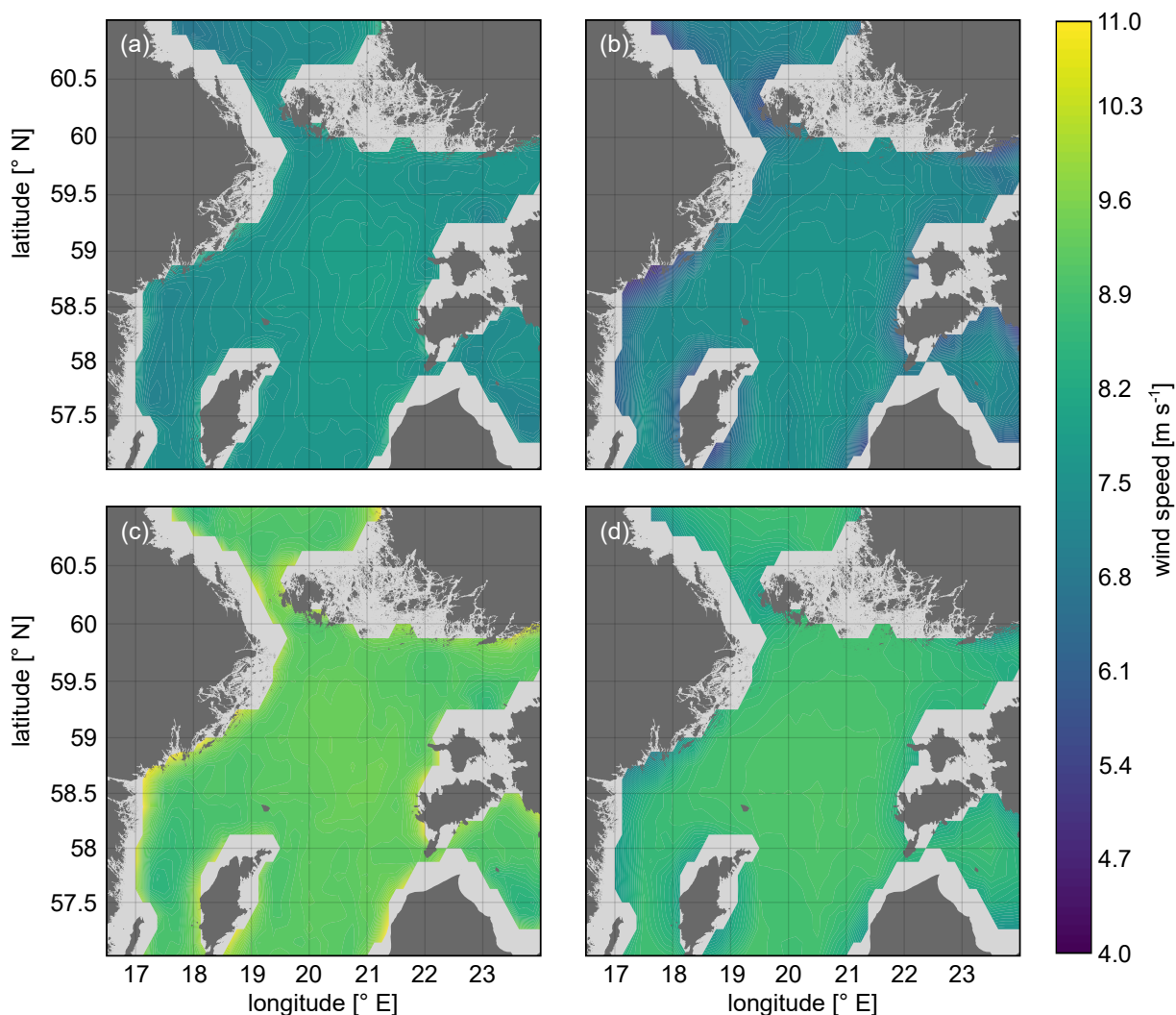


Figure 9. Mean wind speed for the campaign period at 10 m (upper panels) and 100 m (bottom panels) for ASCAT (left panels) and ERA5 (right panels).

Figure 10a illustrates the disparity in wind speed between ASCAT and ERA5 at 10 m and 100 m, plotted as a function of the distance to the shore (calculated from the centre of each grid box). Additionally, probability distribution of the wind speed difference for the two datasets at the aforementioned heights is presented in Fig. 10b. As can be observed, there is a clear correlation between the distance to shore and the agreement of ASCAT and ERA5 observable at both heights. Generally, ASCAT overestimates ERA5 in the majority of the grid points, with this overestimation being higher closer to the coast and for the 100 m level rather than 10 m level. This discrepancy in the nearshore areas can be explained by the combination of too high wind speeds retrieved by ASCAT due to coastal contamination and ERA5's inability to properly resolve the coastal atmospheric phenomena and its coarse horizontal resolution that leads to the omission of the flow phenomena variations caused by the small



350 islands present in this coastal regions. When moving further offshore (more than around 40 km), this overestimation stabilizes, converging to more consistent estimates away from the influence of land and coastal effects and reaching mean difference values of around 0.2 m s^{-1} and 0.4 m s^{-1} at 10 m and 100 m height, respectively,

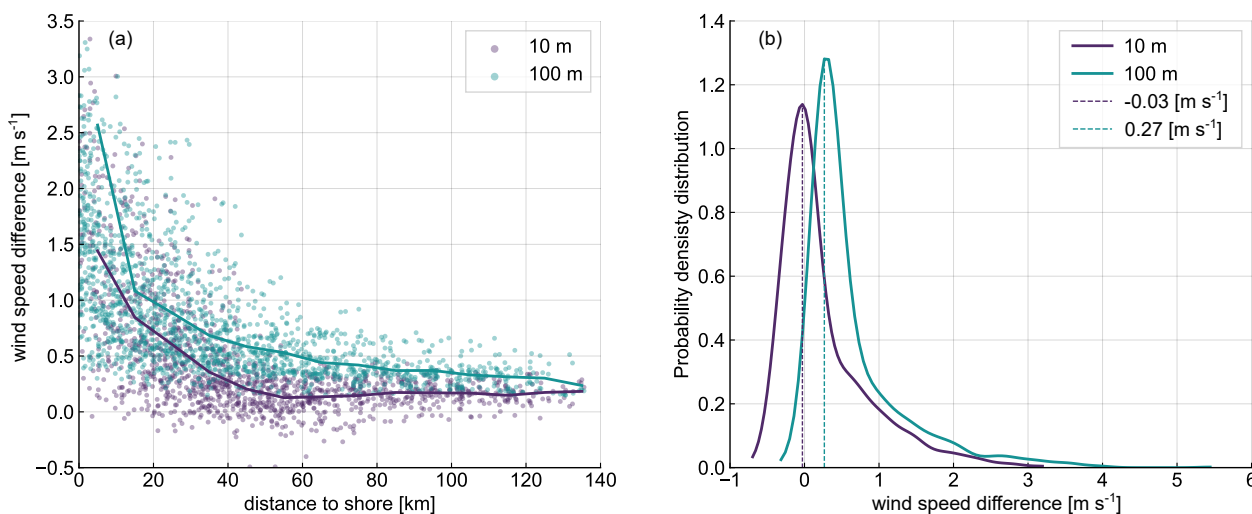


Figure 10. (a) Wind speed difference at 10 and 100 m for ASCAT minus ERA5 at 10 and 100 m as a function of the distance to the shore. (b) Probability density distribution of the wind speed difference at 10 and 100 m for ASCAT minus ERA5. The dashed lines mark the maximum of each of the distribution.

As observed in Fig. 10b, the 10 m height error density distribution is approximately centred at the zero bias point, whereas the distribution at 100 m is slightly positively biased, highlighting the consistent overestimation of wind speed from ASCAT at this height. Nonetheless, the majority of grid points exhibit wind speed differences below $\pm 1 \text{ m s}^{-1}$. As previously discussed, wind speed differences above this threshold correspond to those to near-shore grid points. A similar error distribution was observed in Hasager et al. (2020), when comparing ASCAT and the Weather Research and Forecast (WRF) model over the European seas.

3.3 Comparison against ship-based lidar measurements

360 The overall mean profiles obtained for each of the employed datasets and averaged along the entire ship route are presented in Fig. 11a. Additionally, the mean wind profiles are shown for each of the six locations defined in Fig. 6. The non-stability corrected logarithmic profiles are included for comparison (i.e. term Ψ_m^* from Eq. (4) set to zero).

As can be observed, the accuracy of the overall mean profiles depends on the height and dataset considered. Compared to the lidar data, ERA5 consistently underestimates the wind speed by approximately 0.5 m s^{-1} throughout the entire profile, which aligns with the findings of Rubio et al. (2022). Conversely, the overall mean profile bias of the ASCAT profile is constantly positive (ASCAT overestimation), with magnitude depending on the considered height. Both ERA5 and lidar profiles exhibit a similar shear within the height range covered by the lidar measurement, ranging from 8.4 m s^{-1} to 9.6 m s^{-1} in the case of

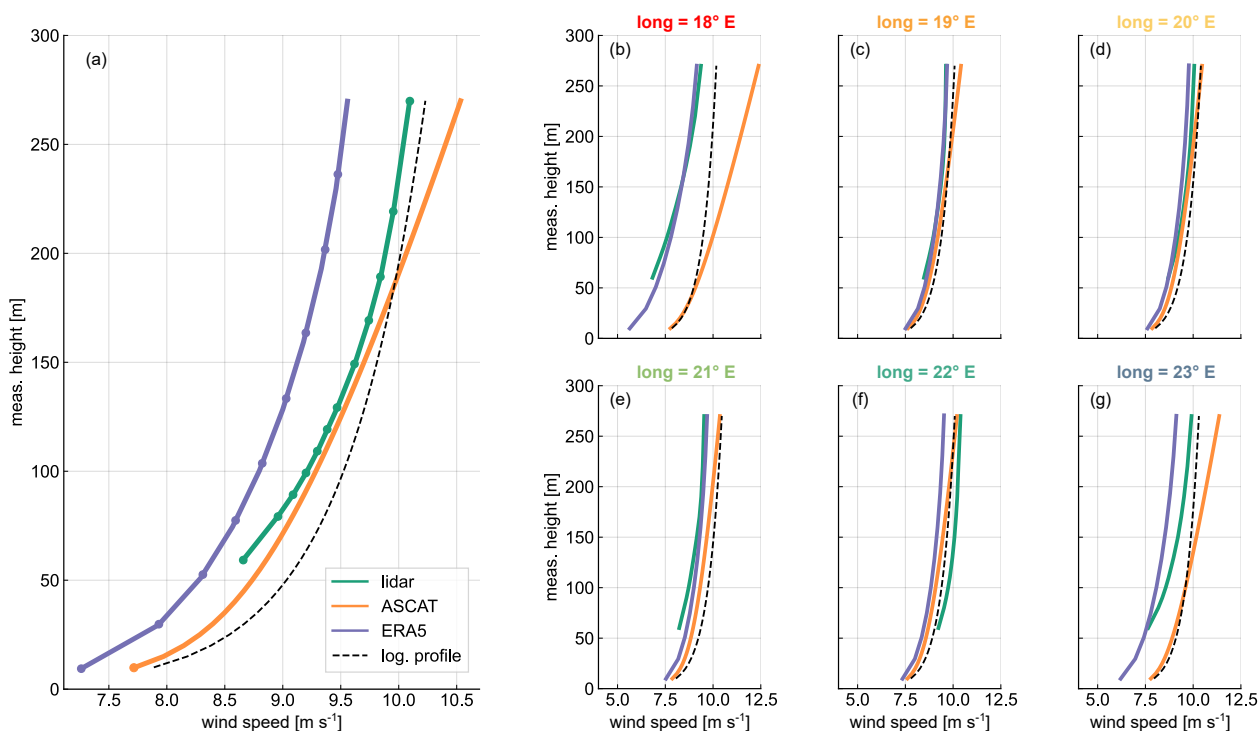


Figure 11. (a) Mean profiles for the three datasets averaged along the whole ship route. The vertical levels with available data/measurements are indicated with circular markers for each dataset. (b - g) Mean profiles for the three datasets at the six evaluated positions. In every panel, the logarithmic profile (non-stability corrected) is indicated by the black dashed line.

ERA5 and from 8.7 m s^{-1} to 10.0 m s^{-1} in the case of the lidar. In contrast, the ASCAT profile struggles to characterize the shear outside the surface layer, with wind speeds ranging from 8.9 m s^{-1} at 60 m height to 10.5 m s^{-1} at 270 m. The ASCAT bias becomes increasingly pronounced above 200 m height, and above this threshold, the logarithmic profile outperforms the stability corrected profile. This is due to the fact that these heights are well beyond the range of applicability of the extrapolation methodology employed (Kelly and Gryning, 2010).

Although the ASCAT wind profiles on average appear to outperform ERA5 in terms of overall accuracy, Figs. 11b-g reveal that the superiority of the datasets varies depending on the considered location. In the case of the harbour locations, ERA5 significantly outperforms ASCAT profiles, which exhibit excessively high wind values even at 10 m height, highlighting the influence of coastal contamination at these sites. Additionally, it is striking to observe the substantial deviation of the ASCAT stability corrected profiles from the logarithmic profiles, particularly at heights above 50-100 m, as a consequence of a stability distribution that is not representative enough of these specific sites. For the remaining locations, both datasets demonstrate excellent and comparable agreement with the lidar wind profile.

A statistical analysis of the wind speed deviation between ASCAT and ERA5 with regards to the lidar observations ($\Delta U_{\text{ASCAT}} = U_{\text{ASCAT}} - U_{\text{lidar}}$ and $\Delta U_{\text{ERA5}} = U_{\text{ERA5}} - U_{\text{lidar}}$) is presented in Fig. 12 in the form of a box plot. Each box plot is calculated con-



385 sidering the wind speed difference for all the grid boxes with lidar data along the whole route of the ship. The black line
corresponds to the median, the coloured box marks the 25th and 75th percentile, and the whiskers indicate the data extremes
calculated as 1.5 times the interquartile range. Outliers outside the whiskers are hidden to maintain clarity and readability. The
continuous lines represent the root mean square error (RMSE) of the wind speed difference between the gridded dataset and
the lidar.

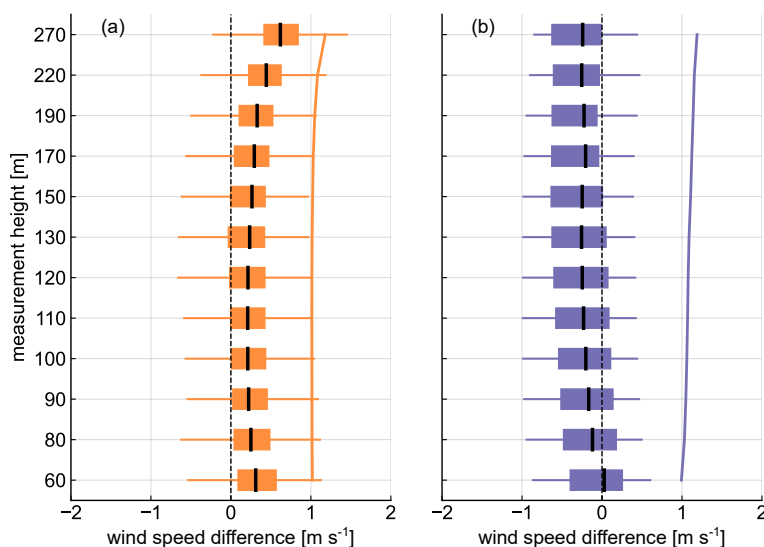


Figure 12. Box plots of the wind speed difference from ASCAT (a) and ERA5 (b) minus the lidar. The coloured boxes extend from the first to the third quartiles of the data and the medians are indicated by black lines. The whiskers extend to the data extremes, defined as a distance of 1.5 times the interquartile range (IQR) above and below the upper and lower quartiles, respectively. The solid lines indicate the RMSE between the gridded datasets and the lidar.

Both datasets show a similar absolute median in the central part of the profile, with median values of around $\pm 0.2 \text{ m s}^{-1}$ in the height range between 90 to 150 m height. However, ERA5 consistently underestimates the wind speed throughout the entire profile, while ASCAT overestimates it at all heights, with the overestimation increasing rapidly above 150 m. Within the
390 upper part of the profile, ERA5 appears to outperform ASCAT, which presents median values rapidly growing with height. The
RMSE analysis reveals similar results for both datasets, with values around 1 m s^{-1} along the profile. Nevertheless, while the
RMSE progressively increases for ERA5, it remains nearly constant up to 190 m for ASCAT and then rapidly increases with
height. The smaller size of the ASCAT boxes in Fig. 12 indicates a narrower spread of wind speed differences compared to
ERA5. However, the longer whiskers suggest a wider range of values beyond the central 50 % of the data, indicating a higher
395 occurrence of outliers associated with excessively high wind speeds near the shore locations.

In order to evaluate the accuracy of ASCAT and ERA5 wind profiles across the different areas covered by the ship route, Fig. 13 illustrates the wind speed differences between these datasets and the lidar profiles for all the grid boxes along the ship track. As can be observed, both datasets show a better performance in regions located further away from the shore, which is



400 evident from the concentration of outliers (points falling outside the confidence intervals) in these areas. This observation holds true for all three presented elevation levels, with only minor variations in the trend. Notably, the western area of the ship route exhibits the widest errors for both ASCAT and ERA5, with maximum differences exceeding 3 m s^{-1} at all elevation levels. This indicates that wind speed estimation in this region is particularly challenging for both datasets due to the intricate topography in the area.

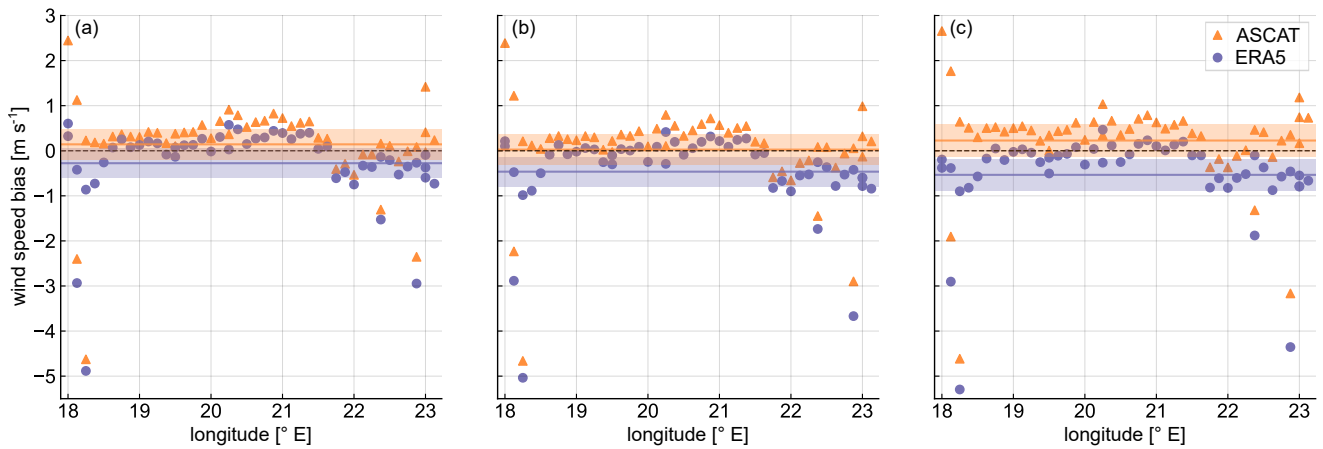


Figure 13. Wind speed bias ($\Delta U_{\text{ASCAT}} = U_{\text{ASCAT}} - U_{\text{lidar}}$ and $\Delta U_{\text{ERA5}} = U_{\text{ERA5}} - U_{\text{lidar}}$) along the different grid boxes depending on their longitude coordinate at 60 m (a), 150 m (b), and 220 m (c) height. The mean biases along the whole ship route are represented by solid lines and the 95 % confidence interval is indicated by the shadowed areas.

The mean differences vary depending on the dataset and the elevation considered, highlighting the different shear resemble
 405 obtained from each of the datasets and their different representation of the wind profiles. ERA5 shows a smaller mean difference of -0.25 m s^{-1} at 60 m, while reaching a maximum value of -0.5 m s^{-1} at 220 m. In the case of ASCAT, the smaller mean difference happens at the intermediate height level, whereas the highest difference can be found also at 220 m height.

It can be noticed that, although ERA5 usually underestimates the wind speed, this is more pronounced at higher elevations and in the eastern part of the ship track. In contrast, ASCAT mainly overestimates compared to the lidar measurements.

410 A final quantification of the accuracy of the gridded datasets compared to the lidar measurements is presented in Fig. 14. Here, the normalized root mean squared error (nRMSE) across all lidar measurement heights is calculated for each compared grid box. The calculation of the nRMSE is expressed in the equations below for ASCAT and ERA5:

$$nRMSE_{\text{ASCAT}} = \frac{\sqrt{\frac{1}{n} \sum_{i=1}^n (U_{\text{ASCAT},i} - U_{\text{lidar},i})^2}}{\bar{U}_{\text{lidar}}} \quad (7)$$

$$nRMSE_{\text{ERA5}} = \frac{\sqrt{\frac{1}{n} \sum_{i=1}^n (U_{\text{ERA5},i} - U_{\text{lidar},i})^2}}{\bar{U}_{\text{lidar}}} \quad (8)$$



415 where n represents the 12 measurements levels of the lidar, U corresponds to the wind speed at the i -th height for each dataset, and \bar{U}_{lidar} is the mean lidar speed averaged across the entire profile.

As can be observed, both datasets present a good agreement in the area of the basin and higher errors in the near shore longitudes. When comparing the two datasets, ERA5 shows a smaller nRMSE in the majority of the studied region, except in the Eastern area near the harbour in Hanko. When comparing the bias and nRMSE shown by the two datasets, the average
420 absolute bias across the entire region is smaller for ASCAT compared to ERA5 at the three heights considered (see Fig. 13). Differently, as can be observed in Fig. 14, most of the locations reveal a smaller nRMSE for ERA5 than for ASCAT. This suggest a higher precision of ERA5, consistently underestimating the observed wind profiles. In contrast, ASCAT's errors exhibit a higher variability - while most grid points overestimate the profiles, few points present a pronounced underestimation. Additionally, as seen in Fig. 12, including higher heights in the consideration for calculating the nRMSE heavily penalizes the
425 performance of the satellite profiles.

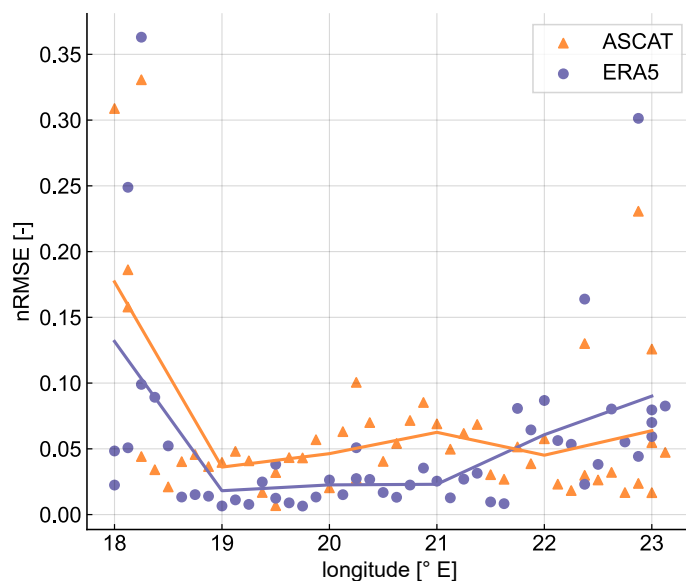


Figure 14. Normalized root mean squared error calculated along the whole profiles for each of the grid boxes. The solid lines represent the binned mean nRMSE calculated using longitude bins of 1°.

4 Discussion

The objective of this study has been to evaluate the accuracy of ASCAT-derived wind speed profiles for the characterization of offshore wind resources at turbine operating heights in the Northern Baltic Sea. Initially, ASCAT winds were compared against the ERA5 reanalysis dataset, the latter frequently serving as a fallback for offshore wind characterization in the absence of in



430 situ measurements. Subsequently, the analysis incorporated a comparison of both gridded datasets against in situ observations obtained from an novel ship-based lidar campaign.

To extrapolate ASCAT wind data, the long-term stability correction methodology formulated by Kelly and Gryning (2010) was employed. This methodology uses the mean ASCAT values for the campaign duration at 10 m altitude in conjunction with atmospheric stability information derived from ERA5. It is noteworthy that previous studies (Optis et al., 2021) have indicated
435 that machine learning-based techniques for extrapolating satellite winds could surpass the long-term correction method employed herein. However, the limited amount of data available over the campaign period hinders the implementation of such data-driven approaches.

One of the main constraints of the long-term extrapolation technique is the requisite for a substantive characterization of the atmospheric stability throughout the comparison period. Consequently, an examination was conducted to assess the im-
440 pact of stability information on ASCAT profile derivation by considering two distinct strategies: collocated and full campaign approaches. The methodology revealed a remarkable congruence between these two approaches across most of the area examined, thus underscoring the robustness of the methodology. However, coastal areas exhibited higher discrepancies, where the collocated approach displayed underestimations of wind speed reaching up to 0.4 m s^{-1} . This divergence can be attributed to the limited availability of valid wind speed measurements in the collocated approach, the constraints of considering atmospheric
445 conditions solely during morning and evening hours, and the generic definition of the empirical constants C_{\pm} required for the calculation of the theoretical stability distributions at each site. Different studies have applied different values of these constant according to the observed stability conditions (Kelly and Gryning, 2010; Badger et al., 2016; Optis et al., 2021). Therefore, further efforts need to be done in order to define a reliable and standard methodology facilitating the definition of the optimal value of these constants according to the specific stability conditions of the site under evaluation.

450 The comparison between ASCAT and ERA5 winds revealed a good agreement between the two datasets. However, significant disparities are evident in near-shore grid points. These discrepancies can be attributed to the intrinsic challenges that both datasets encounter in accurately capturing wind patterns within regions characterized by complex topography. For ERA5, limitations in simulating coastal atmospheric dynamics, such as land-sea breezes and low-level jets, as well as its relatively coarse resolution, prevent the accurate representation of flow effects induced by small islands and rocky islets, prolific in coastal
455 regions considered in this study (Dörenkämper et al., 2015; Gualtieri, 2021). In contrast, satellite measurements proximate to shorelines are susceptible to coastal contamination, occasioned by different factors such as waves breaking and surface slicks (Johannessen, 2005; Kudryavtsev, 2005), and resulting in anomalously high wind measurements. A comparative analysis of mean wind speeds further offshore revealed improved congruity in grid cells situated beyond 40 km from the coastline, with biases stabilizing at approximately 0.2 m s^{-1} and 0.4 m s^{-1} at 10 m and 100 m altitudes, respectively. The application of high-
460 resolution satellite technologies, such as synthetic aperture radar (SAR), could enhance the resolution of coastal wind speed gradients thanks to their finer horizontal resolution (de Montera et al., 2022).

The discrepancies of the two datasets are also highlighted in the coastal regions when compared against the ship-based lidar measurements. Both show highest bias in the longitudes corresponding to the harbour locations, this is, in longitudes further west from 18.5° E and further east from 22.5° E , characterized by a more complex topography. Excluding these nearshore



465 locations, the mean nRMSE along the whole profiles is reduced from 0.07 to 0.05 in the case of ASCAT, and from 0.06 to
0.03 for ERA5. Analogous observations were documented by Takeyama et al. (2019), wherein a comparison of ASCAT data
and Weather Research and Forecasting (WRF) simulations against in situ measurements in the vicinity of the Japanese coast
evinced significantly reduced errors beyond 25 km from the shore.

When comparing the mean profiles of the three datasets, ASCAT exhibited a closer similarity to the lidar wind profile
470 than ERA5. This was particularly pronounced at altitudes ranging from 100 to 150 m. Conversely, ERA5 manifested superior
performance in capturing wind shear across the profile, exhibiting a more consistent bias relative to lidar measurements. This
is consistent with results from previous work in the Southern Baltic Sea (Rubio et al., 2022). The differences between ERA5
and lidar profiles can be elucidated by the different temporal and spatial scales resolved by these datasets, as the lidar is able
to resolve short-term wind variability that may lead to higher mean speeds along the profile. When looking into different
475 locations, the notorious overestimation suffered by ASCAT is evident, with notable errors already at the lower elevations, and
a pronounced amplification in errors as altitude increases. Particularly beyond 190 m, both the bias and RMSE increase rapidly
with height. In contrast to the MOST stability correction approach, the long-term correction approach can be deployed above
the surface layer. The findings of this study indicate a good performance within the lower 200 m of the atmosphere. However, it
must be noticed that the scope of the application depends on the specific atmospheric stability conditions of the location under
480 scrutiny, as well as the period of comparison.

One distinct aspect of the ship-based lidar campaign conducted onboard a ferry ship is the near-constant correlation between
the ship's position and the time of day. Therefore, and similarly to the discretized temporal resolution of ASCAT observations,
the derivation of a complete diurnal wind speed cycle from these measurements at the specific areas covered by the vessel route
is not feasible. Consequently, the mean values derived from lidar measurements may exhibit biases that vary depending on the
485 time slots during which measurements were acquired at particular locations.

Finally, it is imperative to highlight that although the disparities in wind speeds between ASCAT and ERA5 relative to lidar
are generally small in far-offshore regions, their cumulative impact over a large-scale wind energy project can still have relevant
implications for energy production estimates and financial assessments. Therefore, continued efforts to refine both satellite-
based measurements and numerical models are essential to enhance the accuracy of wind resource assessments for offshore
490 wind energy applications. The diverse characteristics and insights into wind patterns derived from satellite-derived observa-
tions, numerical models, and ship-based lidar measurements suggest that an integrative approach, harnessing the collective
strengths of these datasets, could yield substantial gains in the accuracy and reliability of offshore wind statistics derivation.
To this end, several studies have made inroads by generating wind atlases in other regions through the combination of these
datasets (Doubrawa et al., 2015). However, the assimilation of non-stationary measurements and the incorporation of more
495 sophisticated extrapolation methodologies, such as long-term stability correction, could bring further benefits.



5 Conclusions

Satellite-borne scatterometers and numerical models are two potential alternatives for the characterization of offshore wind maps. The long-term stability correction employed in this study demonstrated a strong performance for extrapolating ASCAT winds, yielding to a good agreement compared to the in situ measurements from the ship-based lidar measurements, despite
500 the relatively constrained temporal window of the study.

The fundamental difference of this study from previous literature is the comparison of mean ASCAT extrapolated wind against lidar measurements, encompassing an expansive geographical area, within an increased vertical extension, and through the application of a novel collocating technique. This brings valuable revelations concerning the prospective applicability of ASCAT observations within varying spatial constraints as well as their feasibility at elevated turbine operational altitudes.
505 Moreover, the findings highlight certain inherent challenges when intercomparing datasets with different temporal and spatial characteristics. Such differences may culminate in potential biases amongst datasets, attributed to, for instance, the temporal windows within which measurements are accessible.

Overall, ASCAT derived wind profiles are a valuable asset for portraying offshore wind conditions at turbine operation heights, manifesting a level of accuracy similar to numerical model outputs. However, further research is needed to expand
510 the analysis to other regions and environmental conditions, as well as to assess ASCAT applicability for long-term wind characterization.

Data availability. Data used for this paper were collected from the following sources. Ship-based lidar measurements were provided by Fraunhofer IWES and they are available upon request. The ERA5 data are freely available via the Copernicus Data Storage (CDS): <https://cds.climate.copernicus.eu/cdsapp#!/home>. ASCAT measurements were downloaded via the Copernicus Marine Data Service (CMS): <https://marine.copernicus.eu/>.
515

Author contributions. HR and JG designed and executed the measurement campaign. HR performed the investigation, data processing, analysis and visualization and wrote the manuscript. All authors contributed to the conceptualization and methodology and reviewed the manuscript. JG had a supervisory function.

Competing interests. The authors declare that they have no conflict of interest.

520 *Acknowledgements.* This research received funding from the European Union's Horizon 2020 research and innovation program under the Marie Skłodowska-Curie grant agreement no. 858358 (LIKE – Lidar Knowledge Europe). We would like to express our special thanks to Stena Line for providing us with the opportunity to conduct the campaign onboard the *Stena Gothica* and the Research Institutes of Sweden



RISE for their coordination of the measurement campaign. We would also like to thank the crew of the *Stena Gothica* for their invaluable support during the installation, operation, and dismantling of Fraunhofer IWES's ship-based lidar system.



525 References

- Ahsbahs, T., Maclaurin, G., Draxl, C., Jackson, C. R., Monaldo, F., and Badger, M.: US East Coast synthetic aperture radar wind atlas for offshore wind energy, *Wind Energ. Sci.*, 5, 1191–1210, <https://doi.org/10.5194/wes-5-1191-2020>, 2020.
- Badger, M., Peña, A., Hahmann, A. N., Mouche, A. A., and Hasager, C. B.: Extrapolating Satellite Winds to Turbine Operating Heights, *J. Appl. Meteorol. Clim.*, 55, 975–991, <https://doi.org/10.1175/JAMC-D-15-0197.1>, 2016.
- 530 Bonavita, M., Hólm, E., Isaksen, L., and Fisher, M.: The evolution of the ECMWF hybrid data assimilation system, *Q. J. Roy. Meteorol. Soc.*, 142, 287–303, <https://doi.org/10.1002/qj.2652>, 2016.
- Capps, S. B. and Zender, C. S.: Global ocean wind power sensitivity to surface layer stability, *Geophys. Res. Lett.*, 36, D12 110, <https://doi.org/10.1029/2008GL037063>, 2009.
- Capps, S. B. and Zender, C. S.: Estimated global ocean wind power potential from QuikSCAT observations, accounting for turbine characteristics and siting, *J. Geophys. Res.-Atmos.*, 115, D12 110, <https://doi.org/10.1029/2009JD012679>, 2010.
- 535 Carbon Trust: Carbon Trust Offshore Wind Accelerator Roadmap for the Commercial Acceptance of Floating LIDAR Technology: Technical Report, <https://www.carbontrust.com/our-work-and-impact/guides-reports-and-tools/roadmap-for-commercial-acceptance-of-floating-lidar>, last access: 9 December 2023, 2018.
- Carvalho, D., Rocha, A., Gomez-Gesteira, M., and Silva Santos, C.: Offshore winds and wind energy production estimates derived from ASCAT, OSCAT, numerical weather prediction models and buoys—A comparative study for the Iberian Peninsula Atlantic coast, *Renew. Energ.*, 102, 433–444, <https://doi.org/10.1016/j.renene.2016.10.063>, 2017.
- 540 Chelton, D. B., Ries, J. C., Haines, B. J., Fu, L. L., and Callahan, P. S.: Chapter 1 Satellite Altimetry, *International Geophysics*, 69, 1–183, [https://doi.org/10.1016/S0074-6142\(01\)80146-7](https://doi.org/10.1016/S0074-6142(01)80146-7), 2001.
- Clifton, A., Boquet, M., Des Burin Roziers, E., Westerhellweg, A., Hofsass, M., Klaas, T., Vogstad, K., Clive, P., Harris, M., Wylie, S., Osler, E., Banta, B., Choukulkar, A., Lundquist, J., and Aitken, M.: Remote Sensing of Complex Flows by Doppler Wind Lidar: Issues and Preliminary Recommendations, <https://doi.org/10.2172/1351595>, 2015.
- 545 de Kloe, J., Stoffelen, A., and Verhoef, A.: Improved Use of Scatterometer Measurements by Using Stress-Equivalent Reference Winds, *IEEE J.-STARS*, 10, 2340–2347, 2017.
- de Montera, L., Berger, H., Husson, R., Appelghem, P., Guerlou, L., and Fragoso, M.: High-resolution offshore wind resource assessment at turbine hub height with Sentinel-1 synthetic aperture radar (SAR) data and machine learning, *Wind Energ. Sci.*, 7, 1441–1453, <https://doi.org/10.5194/wes-7-1441-2022>, 2022.
- 550 Dee, D. P., Uppala, S. M., Simmons, A. J., Berrisford, P., Poli, P., Kobayashi, S., Andrae, U., Balmaseda, M. A., Balsamo, G., Bauer, P., Bechtold, P., Beljaars, A. C. M., van de Berg, L., Bidlot, J., Bormann, N., Delsol, C., Dragani, R., Fuentes, M., Geer, A. J., Haimberger, L., Healy, S. B., Hersbach, H., Hólm, E. V., Isaksen, L., Kållberg, P., Köhler, M., Matricardi, M., McNally, A. P., Monge-Sanz, B. M., Morcrette, J.-J., Park, B.-K., Peubey, C., de Rosnay, P., Tavolato, C., Thépaut, J.-N., and Vitart, F.: The ERA-Interim reanalysis: configuration and performance of the data assimilation system, *Q. J. Roy. Meteorol. Soc.*, 137, 553–597, <https://doi.org/10.1002/qj.828>, 2011.
- 555 Dörenkämper, M., Optis, M., Monahan, A., and Steinfeld, G.: On the Offshore Advection of Boundary-Layer Structures and the Influence on Offshore Wind Conditions, *Bound.-Lay. Meteorol.*, 155, 459–482, <https://doi.org/10.1007/s10546-015-0008-x>, 2015.
- Doubrawa, P., Barthelmie, R. J., Pryor, S. C., Hasager, C. B., Badger, M., and Karagali, I.: Satellite winds as a tool for offshore wind resource assessment: The Great Lakes Wind Atlas, *Remote Sens. Environ.*, 168, 349–359, <https://doi.org/10.1016/j.rse.2015.07.008>, 2015.
- 560



- E.U. Copernicus Marine Service Information (CMEMS). Marine Data Store (MDS): Global Ocean Daily Gridded Sea Surface Winds from Scatterometer, <https://doi.org/10.48670/moi-00182>, last access: 23 June 2023.
- Global Wind Energy Council: Global Offshore Wind Report 2022, <https://gwec.net/gwecs-global-offshore-wind-report/>, last access: 9 December 2023, 2022.
- 565 Gottschall, J., Gribben, B., Stein, D., and Würth, I.: Floating lidar as an advanced offshore wind speed measurement technique: current technology status and gap analysis in regard to full maturity, *Wiley Interdiscip. Rev.: Energ. Environ.*, 6, e250, <https://doi.org/10.1002/wene.250>, 2017.
- Gottschall, J., Catalano, E., Dörenkämper, M., and Witha, B.: The NEWA Ferry Lidar Experiment: Measuring Mesoscale Winds in the Southern Baltic Sea, *Remote Sens.*, 10, 1620, <https://doi.org/10.3390/rs10101620>, 2018.
- 570 Gualtieri, G.: Reliability of ERA5 Reanalysis Data for Wind Resource Assessment: A Comparison against Tall Towers, *Energies*, 14, 4169, <https://doi.org/10.3390/EN14144169>, 2021.
- Hasager, C. B., Badger, M., Peña, A., Larsén, X. G., and Bingöl, F.: SAR-Based Wind Resource Statistics in the Baltic Sea, *Remote Sens.*, 3, 117–144, <https://doi.org/10.3390/rs3010117>, 2011.
- Hasager, C. B., Hahmann, A. N., Ahsbahs, T., Karagali, I., Sile, T., Badger, M., and Mann, J.: Europe's offshore winds assessed with synthetic aperture radar, ASCAT and WRF, *Wind Energ. Sci.*, 5, 375–390, <https://doi.org/10.5194/wes-5-375-2020>, 2020.
- 575 Hatfield, D., Hasager, C. B., and Karagali, I.: Comparing Offshore Ferry Lidar Measurements in the Southern Baltic Sea with ASCAT, FINO2 and WRF, *Remote Sens.*, 14, 1427, <https://doi.org/10.3390/rs14061427>, 2022.
- Hatfield, D., Hasager, C. B., and Karagali, I.: Vertical extrapolation of Advanced Scatterometer (ASCAT) ocean surface winds using machine-learning techniques, *Wind Energ. Sci.*, 8, 621–637, <https://doi.org/10.5194/wes-8-621-2023>, 2023.
- 580 Hersbach, H.: CMOD5.N: A C-band geophysical model function for equivalent neutral wind, <https://doi.org/10.21957/mzcfm6jfl>, 2008.
- Hersbach, H., Stoffelen, A., and de Haan, S.: An improved C-band scatterometer ocean geophysical model function: CMOD5, *J. Geophys. Res.-Atmos.*, 112, 1965, <https://doi.org/10.1029/2006JC003743>, 2007.
- Hersbach, H., Bell, B., Berrisford, P., Hirahara, S., Horányi, A., Muñoz-Sabater, J., Nicolas, J., Peubey, C., Radu, R., Schepers, D., Simmons, A., Soci, C., Abdalla, S., Abellan, X., Balsamo, G., Bechtold, P., Biavati, G., Bidlot, J., Bonavita, M., Chiara, G., Dahlgren, P., Dee, D., Diamantakis, M., Dragani, R., Flemming, J., Forbes, R., Fuentes, M., Geer, A., Haimberger, L., Healy, S., Hogan, R. J., Hólm, E., Janisková, M., Keeley, S., Laloyaux, P., Lopez, P., Lupu, C., Radnoti, G., Rosnay, P., Rozum, I., Vamborg, F., Villaume, S., and Thépaut, J.-N.: The ERA5 global reanalysis, *Q. J. Roy. Meteorol. Soc.*, 146, 1999–2049, <https://doi.org/10.1002/qj.3803>, 2020.
- 585 Högström, U., Smedman, A.-S., and Bergström, H.: Calculation of Wind Speed Variation with Height over the Sea, *Wind Eng.*, 30, 269–286, <https://doi.org/10.1260/030952406779295480>, 2006.
- 590 International Renewable Energy Agency: Renewable Energy Capacity Statistics 2023, ISBN 978-92-9260-525-4, 2023.
- Johannessen, J. A.: On radar imaging of current features: 2. Mesoscale eddy and current front detection, *J. Geophys. Res.-Atmos.*, 110, 245, <https://doi.org/10.1029/2004JC002802>, 2005.
- Karagali, I., Peña, A., Badger, M., and Hasager, C. B.: Wind characteristics in the North and Baltic Seas from the QuikSCAT satellite, *Wind Energy*, 17, 123–140, <https://doi.org/10.1002/we.1565>, 2014.
- 595 Karagali, I., Hahmann, A. N., Badger, M., Hasager, C., and Mann, J.: New European wind atlas offshore, *J. Phys. Conf. Ser.*, 1037, 052007, <https://doi.org/10.1088/1742-6596/1037/5/052007>, 2018.
- Kelly, M. and Gryning, S.-E.: Long-Term Mean Wind Profiles Based on Similarity Theory, *Bound.-Lay. Meteorol.*, 136, 377–390, <https://doi.org/10.1007/s10546-010-9509-9>, 2010.



- Kudryavtsev, V.: On radar imaging of current features: 1. Model and comparison with observations, *J. Geophys. Res.-Atmos.*, 110, 10 529, <https://doi.org/10.1029/2004JC002505>, 2005.
- 600 Lange, B., Larsen, S., Højstrup, J., and Barthelmie, R.: The Influence of Thermal Effects on the Wind Speed Profile of the Coastal Marine Boundary Layer, *Bound.-Lay. Meteorol.*, 112, 587–617, <https://doi.org/10.1023/B:BOUN.0000030652.20894.83>, 2004.
- Lindsley, R. D., Blodgett, J. R., and Long, D. G.: Analysis and Validation of High-Resolution Wind From ASCAT, *IEEE Trans. Geosci. Remot Sens.*, 54, 5699–5711, <https://doi.org/10.1109/TGRS.2016.2570245>, 2016.
- 605 Martin, S.: An introduction to ocean remote sensing, Cambridge University Press, New York, second edition edn., 2014.
- Optis, M., Bodini, N., Debnath, M., and Doubrawa, P.: New methods to improve the vertical extrapolation of near-surface offshore wind speeds, *Wind Energy, Sci.*, 6, 935–948, <https://doi.org/10.5194/wes-6-935-2021>, 2021.
- Peña, A., Gryning, S.-E., and Hasager, C. B.: Measurements and Modelling of the Wind Speed Profile in the Marine Atmospheric Boundary Layer, *Bound.-Lay. Meteorol.*, 129, 479–495, <https://doi.org/10.1007/s10546-008-9323-9>, 2008.
- 610 Pichugina, Y. L., Brewer, W. A., Banta, R. M., Choukulkar, A., Clack, C. T. M., Marquis, M. C., McCarty, B. J., Weickmann, A. M., Sandberg, S. P., Marchbanks, R. D., and Hardesty, R. M.: Properties of the offshore low level jet and rotor layer wind shear as measured by scanning Doppler Lidar, *Wind Energy*, 20, 987–1002, <https://doi.org/10.1002/we.2075>, 2017.
- Remmers, T., Cawkwell, F., Desmond, C., Murphy, J., and Politi, E.: The Potential of Advanced Scatterometer (ASCAT) 12.5 km Coastal Observations for Offshore Wind Farm Site Selection in Irish Waters, *Energies*, 12, 206, <https://doi.org/10.3390/en12020206>, 2019.
- 615 Rubio, H. and Gottschall, J.: Development of an analytical uncertainty model for ship-based lidar measurements, *J. Phys. Conf. Ser.*, 2362, 012 034, <https://doi.org/10.1088/1742-6596/2362/1/012034>, 2022.
- Rubio, H., Kühn, M., and Gottschall, J.: Evaluation of low-level jets in the Southern Baltic Sea: a comparison between ship-based lidar observational data and numerical models, *Wind Energy, Sci.*, <https://doi.org/10.5194/wes-2022-40>, 2022.
- Savazzi, A. C. M., Nuijens, L., Sandu, I., George, G., and Bechtold, P.: The representation of the trade winds in ECMWF forecasts and reanalyses during EUREC 4 A, *Atmos. Chem. Phys.*, 22, 13 049–13 066, <https://doi.org/10.5194/acp-22-13049-2022>, 2022.
- 620 Smedman, A.-S., Bergström, H., and Grisogono, B.: Evolution of stable internal boundary layers over a cold sea, *J. Geophys. Res.-Atmos.*, 102, 1091–1099, <https://doi.org/10.1029/96JC02782>, 1997.
- Stoffelen, A., Portabella, M., Verhoef, A., Verspeek, J., and Vogelzang, J.: High-Resolution ASCAT Scatterometer Winds Near the Coast, *IEEE Trans. Geosci. Remot Sens.*, 50, 2481–2487, 2008.
- 625 Stoffelen, A., Verspeek, J. A., Vogelzang, J., and Verhoef, A.: The CMOD7 Geophysical Model Function for ASCAT and ERS Wind Retrievals, *IEEE J. Sel. Top. Appl. Earth Obs. Remote Sens.*, 10, 2123–2134, 2017.
- Stull, R. B.: An introduction to boundary layer meteorology, vol. v. 13 of *Atmospheric and oceanographic sciences library*, Springer, [Berlin], 1988.
- Svensson, N.: Mesoscale Processes over the Baltic Sea, Ph.D. thesis, Department for Earth Sciences, Uppsala University, 2018.
- 630 Verhoef, A. and Stoffelen, A.: Validation of ASCAT 12.5-km Winds, 2013.
- Verhoef, A. and Stoffelen, A.: EUMETSAT Advanced Retransmission Service ASCAT Wind Product User Manual: Technical Report, 2019.
- Verspeek, J., Stoffelen, A., Verhoef, A., and Portabella, M.: Improved ASCAT Wind Retrieval Using NWP Ocean Calibration, *IEEE Trans. Geosci. Remot Sens.*, 50, 2488–2494, <https://doi.org/10.1109/TGRS.2011.2180730>, 2012.
- Wind Europe: Scaling up Floating Offshore Wind towards competitiveness, <https://windeurope.org/wp-content/uploads/files/policy/position-papers/20211202-WindEurope-Scaling-up-Floating-Offshore-Wind-towards-competitiveness.pdf>, last access: 09 December 2023, 2021.
- 635



- Witha, B., Dörenkämper, M., Frank, H., García-Bustamante, E., González-Rouco, F., Navarro, J., Schneider, M., Steeneveld, G.-J., Svensson, N., and Gottschall, J.: The NEWA Ferry Lidar Benchmark: Comparing mesoscale models with lidar measurements along a ship route, Wind Energy Science Conference, 17–20 June 2019, Cork, Ireland, <https://doi.org/10.5281/zenodo.3372693>, 2019a.
- 640 Witha, B., Hahmann, A., Sile, T., Dörenkämper, M., Ezber, Y., García-Bustamante, E., González-Rouco, J. F., Leroy, G., and Navarro, J.: WRF model sensitivity studies and specifications for the NEWA mesoscale wind atlas production runs, <https://doi.org/10.5281/zenodo.2682604>, 2019b.
- Wolken-Möhlmann, G. and Gottschall, J.: Ship-based lidar measurement in the wake of an offshore wind farm, J. Phys. Conf. Ser., 555, 012 043, <https://doi.org/10.1088/1742-6596/555/1/012043>, 2014.